Plasmodium falciparum protein phosphatase PP7 is required for early ring-stage development

Avnish Patel[1], Joshua A. Rey[1], Helen R. Flynn[3], Konstantinos Koussis[2], Mark J. Skehel[3], Michael J. Blackman[2,1] and David A. Baker[1]*

1. Department of Infection Biology, London School of Hygiene & Tropical Medicine, London, United Kingdom.

2. Malaria Biochemistry Laboratory, The Francis Crick Institute, London, United Kingdom

3. Proteomics laboratory, The Francis Crick Institute, London, United Kingdom and Department of Infection Biology, London School of Hygiene & Tropical Medicine, London, United Kingdom.

*Corresponding author

david.baker@lshtm.ac.uk

Abstract

We previously reported that the *Plasmodium falciparum* putative serine/threonine protein phosphatase 7 (PP7) is a high confidence substrate of the cAMP-dependent protein kinase (PKA). Here we explore the function of PP7 in asexual *P. falciparum* blood stage parasites. We show that conditional disruption of PP7 leads to a severe growth arrest. We show that PP7 is a calcium-dependent phosphatase which interacts with calmodulin and calcium-dependent protein kinase 1 (CDPK1), consistent with a role in calcium signalling. Notably, PP7 was found to be dispensable for erythrocyte invasion, but was crucial for ring-stage development, with PP7-null parasites arresting shortly following invasion and showing no transition to ameboid forms. Phosphoproteomic analysis revealed that PP7 may regulate dephosphorylation of PKAc substrates, particularly in the presence of Ca^{2+}. Its interaction with

calmodulin and CDPK1 further emphasise a role in calcium signalling, while its impact on early ring development and PKAc substrate phosphorylation underscores its importance in parasite development.

Introduction

Protein phosphorylation is an essential post-translational modification event that is dynamically controlled by the action of protein kinases and protein phosphatases in all eukaryotic cells. The major human malaria pathogen *Plasmodium falciparum* possesses 90 putative protein kinases (Miranda-Saavedra et al., 2012; Ward et al., 2004) and 27 putative protein phosphatases (Wilkes & Doerig, 2008). Genome-wide screens in *P. berghei*, a rodent malaria species, has identified the stage-specific essentiality of kinases and phosphatases (Guttery et al., 2014; Tewari et al., 2010). With the widespread adoption of conditional gene disruption technologies in *Plasmodium*, several of the essential kinases have been further studied for their cell-specific roles (Davies et al., 2020; Dvorin et al., 2010; Ganter et al., 2017; Koussis et al., 2020; Kumar et al., 2017; Patel et al., 2019). By contrast, essential protein phosphatases have remained relatively under-explored (Fréville et al., 2022), yet an improved understanding of their function is a requisite to discerning the global role of protein phosphorylation dynamics in the complex malaria parasite life cycle, and can also inform target-based drug discovery efforts for rational drug design. Previous studies have assigned functions for essential phosphatases to processes late in the asexual blood stage cycle, revealing roles for calcineurin for merozoite host cell attachment (Paul et al., 2015; Philip & Waters, 2015), PP1 in schizont DNA replication and egress (Paul et al., 2020), and NIF4 in merozoite invasion (Zhu et al., 2022). However, to our knowledge no malarial protein phosphatase has been shown to play a role in the early developmental phases of asexual blood stage parasites.

We previously identified 39 potential substrates of the cAMP dependent protein kinase catalytic subunit (PKAc), an essential kinase required for merozoite invasion of host erythrocytes. Phosphosites within these protein substrates were found to be upregulated following disruption of adenylyl cyclase β or PKAc, and correspondingly downregulated following deletion of phosphodiesterase β (Flueck et al., 2019; Patel et al., 2019). Amongst the putative PKAc substrates identified, PP7 was considered of particular interest in our efforts to elucidate the cell signalling events underlying erythrocyte invasion due to its predicted essentiality and its peak transcriptional expression in mature schizonts.

Here we investigate the function of *P. falciparum* PP7. We find it to be indispensable for asexual blood stage parasite growth, and specifically for the development of early ring-stage parasites. We show that PP7 is expressed in late schizont stages, that its activity is Ca^{2+}-dependent, and that it interacts with both calmodulin and the Ca^{2+}-dependent protein kinase CDPK1. Finally, we use global phospho-proteomics to identify sites that are differentially regulated by PP7.

Results

The architecture of PP7 includes calcium-binding domains

PP7 is annotated as a member of the Phospho-Protein Phosphatases (PPP) family (PlasmoDB (Aurrecoechea et al., 2009) PF3D7_1423300). Its overall structure comprises a central predicted serine/threonine protein phosphatase domain (Kamada et al., 2020) flanked by putative Ca^{2+}-binding-related domains: an N-terminal calmodulin binding IQ domain (Jang et al., 2011) and two C-terminal Ca^{2+}-binding EF hands (Heizmann, 2019) (Fig 1A). This architecture is characteristic of members of one of the five sub-families of the phosphoprotein phosphatase (PPP) family, PPEF/PP7, with EF referring to the presence of an EF-hand domain downstream of the phosphatase catalytic domain. Fig S1 shows the

domain structure of the *P. falciparum* PP7 and alignments with orthologues from other eukaryotes (Steele et al., 1992).

P. falciparum PP7 is expressed in mature schizonts and is essential for asexual blood stage parasite growth

To investigate the biological function of PP7 in *P. falciparum* blood stages, we generated a transgenic parasite line (called PP7-HA:loxP) in a manner designed to allow determination of both the subcellular location of PP7 and the consequences of conditional disruption of PP7. The mutant line was generated on the genetic background of a 3D7 *P. falciparum* line that stably expresses dimerisable Cre (DiCre), the Cre-recombinase activity of which is induced in the presence of rapamycin (RAP) (Knuepfer et al., 2017). The PP7 gene was 'floxed' such that treatment with RAP would lead to excision of DNA sequences encoding the phosphatase catalytic domain and all downstream features (Fig 1B). At the same time the gene was also modified by fusion to sequence encoding a C-terminal triple hemagglutinin (HA) epitope tag (Fig 1B).

Successful modification of the PP7 locus in PP7-HA:loxP parasites was verified by PCR (Fig 1B and C) and western blot, which also showed loss of expression following RAP-induced truncation of the tagged PP7-HA (Fig 1D). Immunofluorescence analysis (IFA) of the transgenic line revealed a partly peripheral signal in individual merozoites within mature segmented schizonts (Fig 1E), similar to the pattern observed by co-staining with the inner membrane complex marker glideosome associated protein 45 (GAP45) (Perrin et al., 2018).

To investigate the essentiality of PP7, highly synchronised young ring-stage cultures of PP7-HA:loxP were treated with RAP to induce excision of the sequence encoding the phosphatase catalytic domain at 4 hrs post invasion (Fig 1B), and parasite replication assessed using flow cytometry (Fig 2). RAP-treated PP7-HA:loxP parasites matured normally through the cycle of RAP-treatment (cycle 0), but then underwent severe growth arrest early in the next cycle (cycle 1). Examination of the cycle 1 parasites by Giemsa-staining showed that the development of early ring stages was adversely affected in RAP-treated PP7-null parasites, with an accumulation of pycnotic parasites that appeared immediately after invasion. In contrast, new rings of control PP7-HA:loxP parasites treated with vehicle only (DMSO) developed normally and went on to form schizonts (Fig 2 inset). It was concluded that PP7 is essential for asexual blood stage survival and that it plays a role in formation of ring-stage parasites soon after erythrocyte invasion.

PP7 is a calcium-dependent phosphatase

Since the domain structure of *P. falciparum* PP7 includes putative domains involved in calcium sensing, we sought to investigate whether PP7 is a calcium-dependent phosphatase. For this, we isolated PP7 from extracts of PP7-HA:loxP parasites by immuno-precipitation with magnetic anti-HA conjugated beads (Fig 3A). The immobilized PP7 was then examined for phosphatase activity in the absence or presence of Ca^{2+} or chelating agents. As shown in in Fig 3B, PP7 displayed phosphatase activity which was strongly enhanced by the presence of Ca^{2+} and inhibited by calcium chelators (Fig 3B). These results indicate that parasite-derived PP7 is a functional phosphatase and that its activity is Ca^{2+} dependent.

PP7 interacts with calmodulin and CDPK1

The observed calcium-dependence of PP7 activity raised the possibility that it may play a role in calcium-mediated signalling. To evaluate this and to gain further mechanistic insight into the role of PP7, we sought to identify potential PP7-interacting partner proteins. For this, immuno-precipitated material from PP7-HA:loxP schizonts was analysed by mass spectrometry to identify co-purifying protein species with and without the presence of additional Ca^{2+}. As shown in Fig 4A and Supplementary Table 1, this analysis revealed that PP7 interacts with calmodulin and calcium-dependent protein kinase 1 (CDPK1), an enzyme involved in parasite invasion and development (Kumar et al., 2017). This finding was confirmed by western blot analysis of PP7 immuno-precipitates using a CDPK1-specific antibody (Fig 4B). The mass spectrometric analysis also identified a conserved protein of unknown function (PF3D7_0423300) that was only enriched in the absence of added Ca^{2+}, suggesting a calcium-dependent interaction of PP7 and PF3D7_0423300. Collectively, these results were interpreted as indicating a role for PP7 in calcium-mediated signalling in *P. falciparum*.

PP7 is not required for invasion but is essential for early ring-stage development

To further investigate how loss of PP7 affects asexual parasite development, we quantified and characterized schizont and resultant ring formation over time in control and RAP-treated (PP7-null) PP7-HA:loxP parasites. This showed no effects of PP7 deletion on the apparent numbers of schizonts and subsequent ring stage formation, as determined by flow cytometry (Fig 5). However, microscopic analysis of Giemsa-stained parasites 2 h post-invasion showed that newly intraerythrocytic PP7-null parasites did not develop post-invasion, instead displaying a predominantly dot-like morphology (Fig 6A). To analyse this ring-stage development defect in more detail we modified the PP7-HA:loxP line to express a cytosolic mNeon-Green marker (Patel et al., 2019), resulting in the PP7-HA-cyto-mNeon:loxP line in which we could observe the morphology of the cell cytosol by green fluorescence in live cells.

Imaging of control or RAP-treated PP7-HA-cyto-mNeon:loxP parasites that had additionally been stained with a membrane marker BODIPY Tr ceramide and DNA stain Hoechst 33342 showed that RAP-treated (PP7-null) parasites formed pycnotic structures that failed to expand, in contrast with the clearly-defined ameboid structures in control parasites (Fig 6B). Together these data indicate a crucial role for PP7 in early ring-stage ameboid development.

PP7 may influence phosphorylation of PKA substrates

We reasoned that as PP7 is a high confidence PKA substrate which possesses phosphatase activity that may be activated by calcium signalling, a process that occurs in parallel with cAMP signalling in merozoites, PP7 may act to regulate phosphorylation of other PKAc substrates. To address this, we used an antibody specific to phosphorylated PKA consensus motifs R, R/K, X, pS/pT (where R is arginine, K is lysine, X is any amino acid and pS or pT denote phosphorylated serine or threonine) to examine control and RAP-treated PP7-HA:loxP schizonts that had either been allowed to undergo rupture to release free merozoites with the associated cytosolic Ca^{2+} elevation, or that had been arrested with the PKG inhibitor compound 2 (C2) to prevent initiation of cytosolic Ca^{2+} elevation(Balestra et al., 2021; Brochet et al., 2014; Pandey et al., 2016). As shown in Fig 7A, loss of PP7 resulted in no detectable change in the intensity of antibody-reactive polypeptides in C2-arrested schizonts, where the egress-associated calcium signalling is absent (Fig 7A). By contrast, in rupturing schizonts and free merozoites, where calcium signalling is present, the absence of PP7 led to a decrease in the intensity of antibody-reactive polypeptides. This result suggests that PP7 phosphatase activity is required for maximal PKAc substrate phosphorylation (Fig 7A).

Loss of PP7 results in phosphoproteomic changes

To gain further insight into the mechanisms through which PP7 controls early ring-stage development, we profiled the PP7-dependent phosphoproteome from schizonts and merozoites of PP7-null and control parasites cultures, reasoning that these are most likely to represent the developmental lifecycle stages in which Ca^{2+}-dependent signalling could plausibly exert control over PP7 activity. Phosphopeptides enriched from trypsin-digested protein extracts of control and RAP-treated PP7-HA:loxP parasites were examined by tandem mass spectrometry using isobaric labelling for quantification. This showed that whilst phosphorylation sites of PP7 were significantly down-regulated in the PP7-null parasites, as expected, phosphosites on only two other proteins showed significant down- or up-regulation: the up-regulated sites were on the protein encoded by PF3D7_1247400 a peptidyl-prolyl cis-trans isomerase FKBP35, whilst the down-regulated sites were on the protein encoded by PF3D7_1221300 a putative EF hand domain-containing protein which was found to be expressed in late schizonts in a transcriptomic study (Toenhake et al., 2018). These results confirmed that loss of PP7 results in a selective set of phosphoproteomic changes in the parasite that could underlie the ring development phenotype.

Discussion

The findings presented in this study shed light on the crucial role of PP7, a biochemically active serine/threonine protein phosphatase, in *P. falciparum* blood stages, expanding our understanding of the signalling machinery of this deadly parasite.

Our data unequivocally demonstrate that PP7 is indispensable for asexual blood stage survival in *P. falciparum*. Conditional disruption of PP7 led to a severe growth arrest, emphasizing its role in early asexual blood stage parasite replication. This aligns with previous findings from a global *P. berghei* knockout screen (Guttery et al., 2014), reinforcing the notion that PP7 plays a conserved and vital role in

Plasmodium species. The striking accumulation of pycnotic parasites in early ring stages upon PP7 disruption led us to investigate and confirm a role in ameboid formation. This amoeboid form has recently been described (Grüring et al., 2011) and remains an understudied aspect of early invaded parasite development.

The discovery of PP7 as a calcium-dependent phosphatase is a significant revelation. The pronounced increase in PP7 activity in the presence of Ca^{2+}, which could be reversed by calcium chelation, implies a role in calcium signalling, which is pivotal during various transitions during the asexual blood stage lifecycle, including erythrocyte invasion and egress (Brochet et al., 2014; Brochet & Billker, 2016; Dvorin et al., 2010; Kumar et al., 2017). Our results suggest that the calcium-dependent phosphatase activity of PP7 plays a crucial role in regulating key calcium-dependent events in the parasite life cycle.

These conclusions are supported by our identification of calmodulin and calcium-dependent protein kinase 1 (CDPK1) as interacting partners of PP7. Calmodulin is a known calcium sensor, and CDPK1 plays a crucial role in parasite invasion and development. The apparent interaction of PP7 with these proteins strongly suggests a role for PP7 in orchestrating crucial calcium-dependent signalling cascades. Given that PP7 is a high confidence PKAc substrate (Patel et al., 2019), it is plausible to suggest that PP7 may act as molecular player in the interaction between the PKAc and calcium-mediated cell signalling pathways in blood stage schizonts. Indeed, cross-talk between these two pathways has been previously observed (Beraldo et al., 2005; Furuyama et al., 2014) but the precise molecular processes governing this remain to be elucidated. We suggest that this role could be fulfilled in part by PP7.

While PP7 was found to be dispensable for erythrocyte invasion, its requirement for early ring-stage development is noteworthy. The developmental arrest observed in PP7-null rings may suggest a crucial role in the organization or maturation of structures critical for the development of newly invaded parasites that contribute to the amoeboid morphology. Interestingly, the *Toxoplasma* orthologue of

PP7, *Tg*PP7, is also essential for parasite replication and virulence *in vivo* (Liang et al., 2022). In contrast to our findings with *P. falciparum* PP7, however, *Tg*PP7 was found to have a role in tachyzoite invasion. This implies the evolutionary co-option of PP7 to suit species-specific roles in apicomplexan invasion and early invaded parasite development. Further work is warranted to elucidate the precise mechanisms underlying these differences.

The observation that PP7 disruption affects phosphorylation of PKAc substrates, especially in the presence of calcium signalling, implies a role in regulating PKAc activity. Given the importance of cAMP and calcium signalling in parasite biology, the modulation of PKAc or PKAr phosphorylation by PP7 is an exciting avenue for future research. How this might occur remains elusive given that we were unable to detect any significantly changed phosphorylation sites could be detected within either PKAc or PKAr in or phospho-proteomic experiments when PP7 was ablated.

The phosphoproteomic profiling of PP7-dependent processes in mature schizonts and merozoites represents a rich dataset for further exploration. We detected just two proteins other than PP7 phosphorylation of which altered significantly upon loss of PP7. The putative EF hand domain-containing protein PF3D7_1221300 is predicted to be non-essential (Zhang et al., 2018), but nonetheless underscores the potential role of PP7 in calcium signaling. The peptidyl-prolyl cis-trans isomerase FKBP35 (PF3D7_1247400) is predicted to be essential (Zhang et al., 2018) and is most highly expressed in the early schizont stage (Toenhake et al., 2018). FK506-binding proteins have been shown to catalyze the cis-trans isomerization of proline imidic peptide bonds (Neye, 2007) and have a role in protein folding (Jo et al., 2015) but little is known of the specific cellular roles in model organisms. The potential role of PP7 in regulation of protein folding processes presents an interesting avenue for future research.

In conclusion, our findings underscore the multifaceted role of PP7 in *P. falciparum* asexual blood stage development. The essentiality of PP7, its calcium-dependent phosphatase activity, and its interactions

with key signalling molecules, together with its role in maximal PKAc substrate phosphorylation in free merozoites, emphasize the importance of PP7 in the cell biology of the parasite. Our work opens new avenues for research into the mechanisms underlying PP7 functions, its contribution to parasite survival, and its potential as a target for anti-malarial drug development.

Acknowledgements

This work was also supported by funding from the Wellcome Trust to DAB (220318/Z/20/Z) and to MJB from the Wellcome Trust (220318/A/20/Z) and the Francis Crick Institute (https://www.crick.ac.uk/) which receives its core funding from Cancer Research UK (CC2129), the UK Medical Research Council (CC2129), and the Wellcome Trust (CC2129).

Materials and Methods

P. falciparum culture and synchronisation

P. falciparum erythrocytic stages were cultured in human erythrocytes (National Blood Transfusion Service, UK) and RPMI 1640 medium (Life Technologies) supplemented with 0.5% Albumax type II (Gibco), 50 µM hypoxanthine, and 2 mM L-glutamine at 37^0C and supplied with (gas composition). Synchronous parasite cultures were obtained as described previously (Harris et al., 2005). Briefly, late segmented schizonts were enriched by centrifugation on a 63% Percoll (GE Healthcare) cushion, followed by the addition of fresh erythrocytes to allow invasion for 1–2 h with continuous shaking. Remaining schizonts were then lysed by sorbitol treatment to yield highly synchronous ring-stage cultures. In all cases, induction of DiCre activity when required was by treatment for 2–4 h with 100 nM

rapamycin (RAP; Sigma) as described previously (Collins et al., 2013; Jones et al., 2016). Control parasites were treated with vehicle only (0.1% v/v DMSO).

The PP7-HA:loxP line was generated from the DiCre-expressing 3D7 *P. falciparum* clone (Knuepfer et al., 2017) using SLI (Birnbaum et al., 2017) with a plasmid containing a SERA2loxPint followed by a triple-HA tag and an in frame *Thosea asigna* virus 2A (T2A) ribosomal skip peptide and NeoR cassette with a downstream loxP and PbDT 3'UTR sequences as described previously (Patel et al., 2019). To ensure appropriate recombination to drive gene excision and C-terminal tagging, a re-codonised version of the C-terminal portion of PP7, containing the phosphatase catalytic domain and downstream EF hands, was synthesised commercially (IDT) and inserted downstream of the SERA2loxPint and upstream of the 3×HA tag. The sequence of the ~800 bp upstream homology region is shown in Figure S2A.

Oligonucleotide primer sequences used in diagnostic PCR to detect integration and excision of transgenes, and the sequences of re-codonised regions, are provided below in Tables 1 and 2.

PP7-HA:loxP mNeon was generated by transfection of PP7-HA:loxP with a construct targeting the p230p locus. A linearised donor DNA fragment which inserted mNeon in-frame with a T2A peptide and BSD selection marker when integrated, and a pDC2-based p230p targeting Cas9 gRNA plasmid was co-transfected. Parasites were left to grow for two days post transfection followed by treatment with 5 µg/ml blasticidin (BSD) to select for integrants. After the emergence of BSD-resistant parasites gDNA was screened for correct integration.

Parasite sample preparation and western blot

Parasite extracts were prepared from Percoll-purified schizonts treated with 0.15% w/v saponin to remove erythrocyte material. To solubilise parasite proteins, PBS-washed saponin-treated parasite pellets were resuspended in three volumes of NP-40 extraction buffer (10 mM Tris, 150 mM NaCl, 0.5 mM EDTA, 1% NP40, pH 7.5, with 1× protease inhibitors (Roche). Samples were gently vortexed and incubated on ice for 10 min followed by centrifugation at 12,000g for 10 min at 4°C. For western blot, SDS-solubilised proteins were electrophoresed on 4%-15% Mini-PROTEAN TGX Stain-Free Protein Gels (Bio-Rad) under reducing conditions and proteins transferred to nitrocellulose membranes using a semidry Trans-Blot Turbo Transfer System (Bio-Rad). Antibody reactions were carried out in 1% skimmed milk in PBS with 0.1% Tween-20 and washed in PBS with 0.1% Tween-20. Appropriate horseradish peroxide-conjugated secondary antibodies were used, and antibody-bound washed membranes were incubated with Clarity Western ECL substrate (Bio-Rad) and visualised using a ChemiDoc (Bio-Rad).

Antibodies used for western blots presented in this work were as follows: anti-HA monoclonal antibody (mAb) 3F10 (diluted 1:2,000) (Roche); mouse anti-GAPDH mAb (1:20,000).

Immunofluorescence assays

Thin blood films were fixed with 4% formaldehyde in PBS and permeabilised with PBS containing 0.1% (v/v) Triton X-100. Blocking and antibody binding was performed in PBS 3% BSA w/v at room temperature. Slides were mounted with ProLong Gold Antifade Mountant containing DAPI (Thermo Fisher Scientific). Images were acquired with a NIKON Eclipse Ti fluorescence microscope fitted with a Hamamatsu C11440 digital camera and overlaid in ICY bioimage analysis software. Antibodies used for IFA were as follows: anti-HA monoclonal antibody (mAb) 3F10 (diluted 1:200) (Roche); rabbit anti-GAP45 mAb (1:1000).

Flow cytometry

For growth assays, synchronous ring-stage parasites were adjusted to a 0.1% parasitaemia 1% haematocrit suspension and dispensed in triplicate into six-well plates. Triplicate samples of 100 µL were harvested at days 0, 2, 4 and 6 for each well and fixed with 4% formaldehyde 0.2% glutaraldehyde in PBS. Fixed samples were stained with SYBR green and analysed by flow cytometry.

For the measurement of egress and ring formation of highly synchronized DMSO- and RAP-treated PP7-HA:loxP parasites. A culture of PP7-HA:loxP with a 1 h invasion window was seeded in duplicate at 1% hematocrit at 2% parasitaemia and treated with DMSO or RAP at 4 h post invasion for 2 h. Triplicate 100 µL samples were taken and fixed with 4% formaldehyde 0.2% glutaraldehyde in PBS at hourly intervals from 45-53 h post invasion and at 69 h post invasion the subsequent day. Fixed samples were stained with SYBR green and analysed by flow cytometry. Schizont parasitaemia was determine by gating high signal SYBR positive cells. Ring parasitaemia was determined similarly but by gating low signal SYBR positive cells.

Analysis of PP7 rings stage morphology

A culture of PP7-HA:loxP-mNeonGreen parasites with 1 h synchronicity was split and treated with DMSO or RAP. Cultures were held pre-egress with 1 µM PKG inhibitor (C2) until 50 h post invasion at which point C2 was removed by washing with pre-warmed complete medium. Cultures were left to invade new host cells for 1 h with continuous shaking and staining with BODIPY-Tr ceramide (Thermo). Subsequently a sample of each culture was taken. For Giemsa-stained blood film analysis samples were smeared and fixed with methanol followed by Giemsa staining. For fluorescence microscopy, samples were washed and diluted to 0.1% haematocrit, and placed into a chamber of a poly-L lysine coated Ibidi chamber slide (Ibid) to adhere for 10 minutes at 37 degrees. Adherent cells were then imaged on a

NIKON Eclipse Ti fluorescence microscope fitted with a Hamamatsu C11440 digital camera and overlaid in ICY bioimage analysis software.

Immuno-precipitation

Tightly synchronised schizonts (~45 h post invasion) of PP7-HA:loxP and 3D7DiCre parental parasites were enriched on a 70% Percoll cushion. The schizonts were treated for 3 h with 1 µM C2 (to arrest egress) after which the cultures were treated with 0.15% saponin in PBS containing cOmplete Mini EDTA-free Protease and PhosSTOP Phosphatase inhibitor cocktails (both Roche) for 10 min at 4°C to lyse the host erythrocytes. Samples were washed twice in PBS containing protease and phosphatase inhibitors, snap-frozen and pellets stored at −80°C. Parasite pellets (70-100 µl packed volume) were resuspended in three volumes of NP-40 extraction buffer (10 mM Tris, 150 mM NaCl, 0.5 mM EDTA, 1% NP40, pH 7.5, with 1× protease inhibitors (Roche). Samples were gently vortexed and incubated on ice for 10 min followed by centrifugation at 12,000g for 10 min at 4°C. Clarified lysates were then added to anti-HA antibody-conjugated magnetic beads (Thermo Scientific) which had been equilibrated in NP-40 extraction buffer. Samples were incubated at room temperature for 2 h on a rotating wheel after which beads were precipitated using a magnetic sample rack. The supernatant was removed, and beads washed three times with NP-40 extraction buffer followed by three washes with extraction buffer lacking detergent.

Phosphatase assay

Assays were carried out using the EnzChek Phosphatase Assay Kit (Therno) according to the manufacturer's procedures. Briefly, percoll purified schizont pellets of 50 µl were prepared for PP7-HA:loxP or 3D7DiCre parental parasites. Samples were processed by the methodology for immuno-precipitation. PP7-HA conjugated beads were then resuspended in a total volume of 650 µl of assay

buffer (20 mM Tris, 150 mM NaCl, pH 7.5,). 50 µl of suspended bead slurry was dispensed in triplicate into wells of a 96-well plate for each test condition. 50 µl of reaction buffer containing additives for the conditions tested and difluoro-4-methylumbelliferyl phosphate (DiFMUP) substrate were added, to give a final concentration of 100 µM DiFMUP. A set of control wells were made with the addition of reaction buffer lacking DiFMUP. Plates were incubated at 37°C for 1 h and then read with Ex/Em of 358/455 nm on a spectramax i5 plate reader (company?). Averaged arbitrary fluorescence for each condition was calculated by normalising to the negative control wells.

Mass spectrometry of immuno-precipitated material

Washed beads were resuspended in trypsinisation buffer (50 mM ammonium bicarbonate, 40 mM 2-chloroacetamide and 10 mM Tris-(2-carboxyethyl) phosphine hydrochloride) and samples reduced and alkylated by heated to 70°C for 5 minutes. 250 ng of trypsin was added to the samples and heated at 37°C overnight with gentle agitation followed by filtration using a 0.22 µm Costar® Spin-X® centrifuge tube filter (Sigma). Samples were then run on a LTQ-Orbitrap-Velos mass spectrometer (Thermo Scientific). Search engines, Mascot (http://www.matrixscience.com/) and MaxQuant (https://www.maxquant.org/) were used for mass spectrometry data analysis. The PlasmoDB database was used for protein annotation. Peptide and proteins having minimum threshold of 95% were used for further proteomic analysis and peptide traces analysed using Scaffold5. Enrichment was determined by comparing results from tagged lines with those of immuno-precipitated material from 3D7DiCre parental parasites.

Phosphoproteomics

The phosphoproteomics data presented are from an isobaric labelling experiment. Tightly synchronised, ring-stage PP7-HA:loxP were treated with 100 nM RAP or vehicle only (DMSO) and schizonts (about 45 h old) enriched on an approximately 70% Percoll cushion. The schizonts were treated for 2 h with 1 µM C2

(to arrest egress) and then washed to allow egress for 25 min, after which the cultures were treated with 0.15% saponin in PBS containing cOmplete Mini EDTA-free Protease and PhosSTOP Phosphatase inhibitor cocktails (both Roche) for 10 min at 4°C to lyse the host erythrocytes. Samples were washed twice in PBS containing protease and phosphatase inhibitors, snap-frozen in liquid nitrogen, and pellets stored at −80°C. Parasite pellets were resuspended in 1 mL 8 M urea in 50 mM HEPES, pH 8.5, containing protease and phosphatase inhibitors and 100 U/mL benzonase (Sigma). Proteins were extracted from the pellets using three 15 s bursts with a probe sonicator followed by a 10 min incubation on ice and a 30 min centrifugation at 14,000 rpm at 4°C. Protein content was estimated by a BCA protein assay and a 200 µg aliquot of each sample was taken for further processing. Samples were reduced with 10 mM dithiothreitol for 25 min at 56°C and then alkylated with 20 mM iodoacetamide for 30 min at room temperature. The alkylation reaction was quenched with an additional 10 mM dithiothreitol, and then each sample was diluted with 50 mM HEPES to reduce the urea concentration to <2 M prior to digestion. Proteolytic digestion was carried out by the addition of 4 µg LysC (WAKO) and incubated at 37°C for 2.5 h followed by the addition of 10 µg trypsin (Pierce) and overnight incubation at 37°C. After acidification, C18 MacroSpin columns (Nest Group) were used to clean up the digested peptide solutions and the eluted peptides dried by vacuum centrifugation. Samples were resuspended in 50 mM HEPES and labelled using the 0.8 mg Tandem Mass Tag 10plex isobaric reagent kit (Thermo Scientific) resuspended in acetonitrile. Labelling reactions were quenched with hydroxylamine, and a pool was made of each set of samples. Acetonitrile content was removed from the pooled TMT solution by vacuum centrifugation and then acidified before using a Sep-Pak C18 (Waters) to clean up the labelled peptide pool prior to phosphopeptide enrichment. The eluted TMT-labelled peptides were dried by vacuum centrifugation and phosphopeptide enrichment was subsequently carried out using the sequential metal oxide affinity chromatography (SMOAC) strategy with High Select TiO2 and Fe-NTA enrichment kits (Thermo Scientific). Eluates were combined prior to fractionation with the Pierce High

pH Reversed-Phase Peptide Fractionation kit (Thermo Scientific). The dried TMT-labelled phosphopeptide fractions generated were resuspended in 0.1% TFA for LC-MS/MS analysis using a U3000 RSLCnano system (Thermo Scientific) interfaced with an Orbitrap Fusion Lumos (Thermo Scientific). Each peptide fraction was pre-concentrated on an Acclaim PepMap 100 trapping column before separation on a 50-cm, 75-µm I.D. EASY-Spray Pepmap column over a 3-h gradient run at 40°C, eluted directly into the mass spectrometer. The instrument was run in data-dependent acquisition mode with the most abundant peptides selected for MS/MS fragmentation. Two replicate injections were made for each fraction with different fragmentation methods based on the MS2 HCD and MSA SPS MS3 strategies described. The acquired raw mass spectrometric data were processed in MaxQuant (version 1.6.2.10) for peptide and protein identification; the database search was performed using the Andromeda search engine against the Homo sapiens canonical sequences from UniProtKB (release 2018_05) and *P. falciparum* 3D7 sequences from PlasmoDB (Aurrecoechea et al., 2009). Fixed modifications were set as Carbamidomethyl (C) and variable modifications set as Oxidation (M) and Phospho (STY). The estimated false discovery rate was set to 1% at the peptide, protein, and site levels. A maximum of two missed cleavages were allowed. Reporter ion MS2 or Reporter ion MS3 was appropriately selected for each raw file. Other parameters were used as preset in the software. The MaxQuant output file PhosphoSTY Sites.txt, an FDR-controlled site-based table compiled by MaxQuant from the relevant information about the identified peptides, was imported into Perseus (v1.4.0.2) for data evaluation.

Figure legends

Figure 1

(1A) Cartoon of the predicted *P. falciparum* PP7 protein showing the positions of the individual domains. Amino acid numbers are shown in black. The arrow indicates the point at which the protein product is truncated when the modified locus is excised in the transgenic parasites.

(1B) Schematic representation of the SLI strategy (Birnbaum et al., 2017) used to produce the PP7-HA:loxP DiCre line and resultant RAP-induced disruption of the modified gene. Double-headed arrows represent the regions amplified by PCR in (1C). Red arrowheads, *loxP* sites, yellow lollipops, translational stop codons, white box, phosphatase domain, light blue box, regions of re-codonised sequence (R.R.).

(1C) Diagnostic PCR analysis of genomic DNA (gDNA) from a transgenic PP7 parasite line verifying successful modification of target loci by SLI to produce PP7-HA:loxP. Efficient excision of 'floxed' sequences is observed upon treatment with RAP. Track C represents amplification of a control locus (PKAr) to check gDNA integrity. PCRs 1-4 are represented in the schematic locus in panel 1B. PCR 1 screens for the WT locus, PCR 2 for 5' integration, PCR 3 for the excision of the 'floxed' sequence and PCR 4 for 3' integration. See Table 1 for sequences of all primers used for PCR. Sizes for expected amplification products are as follows: C, control locus (primers 5 and 6) 836 b.p. PCR 1 (primers 7 and 8) 1296 b.p, PCR2 (primers 7 and 9) 3559 b.p, PCR3 (primers 7 and 10) 1362 b.p. (RAP) and PCR 4 (primers 11 and 8) 1013 b.p.

(1D) Western blot analysis of expression (DMSO, control) and ablation (RAP) of PP7-HA from highly synchronous mature schizonts. Expression of GAPDH (PF3D7_1462800) is shown as a loading control.

(1E) IFA analysis showing the diffuse peripheral localisation of PP7-HA and the loss of expression upon RAP treatment (16 h post invasion). Over 99% of all RAP-treated PP7-HA:loxP schizonts examined by IFA showed diminished HA expression in three independent experiments. Scale bar, 2 µm.

Figure 2

Growth curves showing parasitaemia as measured by flow cytometry of PP7-HA:loxP parasites treated with DMSO (vehicle only control, blue) or RAP (red). Means from three independent biological replicates are plotted. Error bars, SD. Inset, Giemsa-stained thin blood films showing ring-stage parasites following egress of synchronous DMSO- and RAP-treated PP7-HA:loxP schizonts. Ring formation occurs in DMSO-treated PP7-HA parasites, parasites did not develop beyond the early ring stage in RAP-treated parasites.

Figure 3

(3A) Western blot showing immunoprecipitation (IP) of PP7-HA from schizont extracts. Black arrow indicates the predicted mass of PP7-HA. Minor lower molecular weight degradation products are seen. Images are representative of two independent biological repeats.

(3B) Phosphatase assay of immuno-precipitated PP7-HA conjugated beads. PP7 conjugated bead conditions are shown in green and control beads from 3D7 DiCre parental schizont lysate immuno-

precipitation are displayed in blue. Results are averages of three independent biological repeats, error bars, SD.

Figure 4

(4A) Mass spectrometric identification of interacting partners of PP7. The right panel shows immuno-precipitation with no added Ca^{2+} ions, left panel shows immuno-precipitation in the presence of additional 2 mM Ca^{2+} (present during detergent extraction, immuno-precipitation and washes). Volcano plot of P values versus the corresponding log2 fold change in abundance compared to 3D7DiCre control samples (Fischer's exact test). Plotted by analysing proteins enriched through IP (panel 3A) by mass spectrometry. Green line indicates p=-2log10 and green dots represent peptides where p<-2log10. Peptides for PP7 were enriched to p<-19log10.

(4B) Western blot analysis of immuno-precipitated PP7:HA-loxP schizont lysates with anti-HA beads, using the HA antibody (upper), the CDPK1 antibody (middle) and the GAPDH antibody (lower) (used as a negative control cytosolic marker to detect potential non-specific binding).

Figure 5

Flow cytometry analysis of ring formation in DMSO- and RAP-treated PP7-HA:loxP parasites treated in the previous cycle. Samples from highly-synchronized cultures treated at the ring stage the cycle prior to invasion and analysis, were taken in triplicate at the stated time intervals post invasion and stained with the DNA stain SYBR green. Samples were analyzed by flow cytometry, and the schizont and ring

parasitemia values determined by gating high-signal and low-signal SYBR-positive cells, respectively. Mean parasitemia values (starting schizontemia adjusted to 2%) from two independent experiments are plotted. Error bars, SD; Insets are smears taken from cultures at 24h post invasion. Scale bars, 5 µm.

Figure 6

PP7 ablation results in arrest of ring-stage parasite development. (A) Tightly synchronized DMSO- or RAP-treated PP7-HA:loxP parasites were arrested with C2 block and subsequently washed and left to invade in fresh pre-warmed medium. After a further 2 h, thin blood smears were taken, and Giemsa stained. Ring-stage parasite morphology was classified by manual counting. A minimum of 100 cells were counted per replicate and scored for morphology, scale bar 2 µm. (B) Tightly synchronized DMSO- or RAP-treated PP7-HA-Cyto-mNeon:loxP parasites were arrested with C2 and subsequently washed and left to invade in fresh pre-warmed medium. Parasites were then stained with BODIPY TR ceramide and Hoechst 3342 to visualise membranes and nuclei respectively. Parasite samples were placed in an Ibid chamber slide and imaged by fluorescence microscopy. A minimum of 40 ring-stage cells were counted per condition and scored for ameboid or pycnotic morphology of parasites, scale bar 2 µm. Mean data are plotted for three independent experiments. Error bars, SD, * $P<0.05$, Student's t test for the comparison of conditions between DMSO and RAP treatments.

Figure 7

(7A) Tightly-synchronized DMSO- or RAP-treated PP7-HA:loxP parasites were arrested with C2 until 48 h PI and half of the sample was harvested for western blot analysis (+C2). The remaining half was washed with pre-warmed medium to remove C2 and left to rupture for 20 min before harvesting (-C2). Samples were analysed for ablation of PP7 and sample loading by probing with anti-HA and GAPDH antibodies

respectively (left panel). A duplicate loading was probed to identify the abundance and patterning of phosphorylated PKA substrate motifs by probing with an anti-phospho PKA substrate antibody, which detects the motif RRXS*/T*, where S* and T* are phosphorylated serine and threonine residues respectively and X is any amino acid. Images are representative of three independent experiments.

(7B) Volcano plot showing the changes in detection of phospho-sites between DMSO- and RAP-treated PP7-HA:loxP. The negative log10 transform of the p-value–derived Welch-corrected t test comparing five DMSO- and five RAP-treated replicates is plotted against the log2-transformed fold change in reporter ion intensity (DMSO/RAP). Significance of $p < 0.05$ is denoted by the horizontal line. Vertical lines indicate –0.7 and 0.7 log2 fold change.

Table 1-primers used in this study

Number	Primer name	Sequence 5'-3'
1	PP7 5HR F	GCGGCCGCAGATCTCTCGAGGGAAGAAAGCGCCTGTACTATG
2	PP7 5HR R	CGAAGTTATTGTATATTATTTTTTTTATTTACAATTAATTTGGTATCTTTG GACTTTTTG
3	PP7 Reco F	GTATATATATATATATTTATATATTTTATATTCTTTTAGATATTAGGAGAC GTTCATGGACAG
4	PP7 Reco R	CAGATCCGCCTGAACCGGATCCATTATTGCTGTATATATATGTAGGTTTG
5	PKAr F	GCGGCCGCAGATCTCTCGAGCCTAAAGTTTATAAGAAAGATGAAAAAG
6	PKAr R	CAGATCCGCCtGAACCGGATCCATTTTCATCAATACAAGTTGTATCCAAA C
7	5' screen F PP7	CAACATTGAAGATGTTGTTATGATATATG
8	3' screen R PP7	GGTGAAATATATTCAGTCGATGC
9	HA R	GCATAGTCAGGAACATCGTAAGG
10	screen L7 myc R	CCGTTCAAATCTTCTTCAGAAATCAAC
11	pL7 3' screen F	CAGCTATGACCATGATTACGCC
12	p230p Int screen F	CTATATGGTATCCAAAACCTTTAAATTATATAGC

13	p230p WT screen R	GAGGAATTTTTAAATATGATATACCTTTATCATTAG
14	p230p 5 Int screen R	CCAATGGCCCCTTTCCGC
15	p230p 3 Int screen F	CTAGCGGCTTGTCGACG

References

Aurrecoechea, C., Brestelli, J., Brunk, B. P., Dommer, J., Fischer, S., Gajria, B., Gao, X., Gingle, A., Grant, G., Harb, O. S., Heiges, M., Innamorato, F., Iodice, J., Kissinger, J. C., Kraemer, E., Li, W., Miller, J. A., Nayak, V., Pennington, C., … Wang, H. (2009). PlasmoDB: a functional genomic database for malaria parasites. *Nucleic Acids Research*, *37*(Database issue). https://doi.org/10.1093/NAR/GKN814

Balestra, A. C., Koussis, K., Klages, N., Howell, S. A., Flynn, H. R., Bantscheff, M., Pasquarello, C., Perrin, A. J., Brusini, L., Arboit, P., Sanz, O., Castaño, L. P. B., Withers-Martinez, C., Hainard, A., Ghidelli-Disse, S., Snijders, A. P., Baker, D. A., Blackman, M. J., & Brochet, M. (2021). Ca2+ signals critical for egress and gametogenesis in malaria parasites depend on a multipass membrane protein that interacts

with PKG. *Science Advances*, *7*(13). https://doi.org/10.1126/SCIADV.ABE5396

Beraldo, F. H., Almeida, F. M., Da Silva, A. M., & Garcia, C. R. S. (2005). Cyclic AMP and calcium interplay as second messengers in melatonin-dependent regulation of Plasmodium falciparum cell cycle. *The Journal of Cell Biology*, *170*(4), 551. https://doi.org/10.1083/JCB.200505117

Birnbaum, J., Flemming, S., Reichard, N., Soares, A. B., Mesén-Ramírez, P., Jonscher, E., Bergmann, B., & Spielmann, T. (2017). A genetic system to study Plasmodium falciparum protein function. *Nature Methods*, *14*(4), 450–456. https://doi.org/10.1038/NMETH.4223

Brochet, M., & Billker, O. (2016). Calcium signalling in malaria parasites. *Molecular Microbiology*, *00*, 1–12. https://doi.org/10.1002/elsc.201200179

Brochet, M., Collins, M. O., Smith, T. K., Thompson, E., Sebastian, S., Volkmann, K., Schwach, F., Chappell, L., Gomes, A. R., Berriman, M., Rayner, J. C., Baker, D. A., Choudhary, J., & Billker, O. (2014). Phosphoinositide Metabolism Links cGMP-Dependent Protein Kinase G to Essential Ca2+ Signals at Key Decision Points in the Life Cycle of Malaria Parasites. *PLoS Biology*, *12*(3). https://doi.org/10.1371/journal.pbio.1001806

Collins, C. R., Das, S., Wong, E. H., Andenmatten, N., Stallmach, R., Hackett, F., Herman, J. P., Müller, S., Meissner, M., & Blackman, M. J. (2013). Robust inducible Cre recombinase activity in the human malaria parasite Plasmodium falciparum enables efficient gene deletion within a single asexual erythrocytic growth cycle. *Molecular Microbiology*, *88*(4), 687–701. https://doi.org/10.1111/mmi.12206

Davies, H., Belda, H., Broncel, M., Ye, X., Bisson, C., Introini, V., Dorin-Semblat, D., Semblat, J. P., Tibúrcio, M., Gamain, B., Kaforou, M., & Treeck, M. (2020). An exported kinase family mediates species-specific erythrocyte remodelling and virulence in human malaria. *Nature Microbiology*, *5*(6), 848–863. https://doi.org/10.1038/S41564-020-0702-4

Dvorin, J. D., Martyn, a C., Patel, S. D., Grimley, J. S., Collins, C. R., Hopp, C. S., Bright, A. T.,

Westenberger, S., Winzeler, E., Blackman, M. J., Baker, D. A., Wandless, T. J., & Duraisingh, M. T. (2010). A plant-like kinase in Plasmodium falciparum regulates parasite egress from erythrocytes. *Science (New York, N.Y.)*, *328*(5980), 910–912. https://doi.org/10.1126/science.1188191

Flueck C, Drought LG, Jones A, Patel A, Perrin AJ, Walker EM, et al. Phosphodiesterase beta is the master regulator of cAMP signalling during malaria parasite invasion. *PLoS Biology*, 17(2). https://doi.org/10.1371/journal.pbio.3000154 532

Fréville, A., Gnangnon, B., Khelifa, A. S., Gissot, M., Khalife, J., & Pierrot, C. (2022). Deciphering the Role of Protein Phosphatases in Apicomplexa: The Future of Innovative Therapeutics? *Microorganisms*, *10*(3). https://doi.org/10.3390/MICROORGANISMS10030585

Furuyama, W., Enomoto, M., Mossaad, E., Kawai, S., Mikoshiba, K., & Kawazu, S. I. (2014). An interplay between 2 signaling pathways: Melatonin-cAMP and IP3–Ca2+ signaling pathways control intraerythrocytic development of the malaria parasite Plasmodium falciparum. *Biochemical and Biophysical Research Communications*, *446*(1), 125–131. https://doi.org/10.1016/J.BBRC.2014.02.070

Ganter, M., Goldberg, J. M., Dvorin, J. D., Paulo, J. A., King, J. G., Tripathi, A. K., Paul, A. S., Yang, J., Coppens, I., Jiang, R. H. Y., & David, A. (2017). *Plasmodium falciparum CRK4 directs continuous rounds of DNA replication during schizogony*. 1–48. https://doi.org/10.1038/nmicrobiol.2017.17

Grüring, C., Heiber, A., Kruse, F., Ungefehr, J., Gilberger, T. W., & Spielmann, T. (2011). Development and host cell modifications of Plasmodium falciparum blood stages in four dimensions. *Nature Communications*, *2*(1). https://doi.org/10.1038/NCOMMS1169

Guttery, D. S., Poulin, B., Ramaprasad, A., Wall, R. J., Ferguson, D. J. P., Brady, D., Patzewitz, E. M., Whipple, S., Straschil, U., Wright, M. H., Mohamed, A. M. A. H., Radhakrishnan, A., Arold, S. T., Tate, E. W., Holder, A. A., Wickstead, B., Pain, A., & Tewari, R. (2014). Genome-wide functional analysis of plasmodium protein phosphatases reveals key regulators of parasite development and

differentiation. *Cell Host and Microbe*, *16*(1), 128–140. https://doi.org/10.1016/j.chom.2014.05.020

Harris, P. K., Yeoh, S., Dluzewski, A. R., O'Donnell, R. A., Withers-Martinez, C., Hackett, F., Bannister, L. H., Mitchell, G. H., & Blackman, M. J. (2005). Molecular identification of a malaria merozoite surface sheddase. *PLoS Pathogens*, *1*(3), 0241–0251. https://doi.org/10.1371/JOURNAL.PPAT.0010029

Heizmann, C. W. (2019). Ca2+-Binding Proteins of the EF-Hand Superfamily: Diagnostic and Prognostic Biomarkers and Novel Therapeutic Targets. *Methods in Molecular Biology (Clifton, N.J.)*, *1929*, 157–186. https://doi.org/10.1007/978-1-4939-9030-6_11

Jang, D. J., Ban, B., & Lee, J. A. (2011). Characterization of Novel Calmodulin Binding Domains within IQ Motifs of IQGAP1. *Molecules and Cells*, *32*(6), 511. https://doi.org/10.1007/S10059-011-0109-4

Jo, G. A., Lee, J. M., No, G., Kang, D. S., Kim, S. H., Ahn, S. H., & Kong, I. S. (2015). Isolation and characterization of a 17-kDa FKBP-type peptidyl-prolyl cis/trans isomerase from Vibrio anguillarum. *Protein Expression and Purification*, *110*, 130–137. https://doi.org/10.1016/J.PEP.2015.02.019

Jones, M. L., Das, S., Belda, H., Collins, C. R., Blackman, M. J., & Treeck, M. (2016). A versatile strategy for rapid conditional genome engineering using loxP sites in a small synthetic intron in Plasmodium falciparum. *Scientific Reports*, *6*(November 2015), 21800. https://doi.org/10.1038/srep21800

Kamada, R., Kudoh, F., Ito, S., Tani, I., Janairo, J. I. B., Omichinski, J. G., & Sakaguchi, K. (2020). Metal-dependent Ser/Thr protein phosphatase PPM family: Evolution, structures, diseases and inhibitors. *Pharmacology & Therapeutics*, *215*. https://doi.org/10.1016/J.PHARMTHERA.2020.107622

Knuepfer, E., Napiorkowska, M., Van Ooij, C., & Holder, A. A. (2017). Generating conditional gene knockouts in Plasmodium - a toolkit to produce stable DiCre recombinase-expressing parasite lines using CRISPR/Cas9. *Scientific Reports*, *7*(1). https://doi.org/10.1038/S41598-017-03984-3

Koussis, K., Withers-Martinez, C., Baker, D. A., & Blackman, M. J. (2020). Simultaneous multiple allelic

replacement in the malaria parasite enables dissection of PKG function. *Life Science Alliance*, *3*(4). https://doi.org/10.26508/LSA.201900626

Kumar, S., Kumar, M., Ekka, R., Dvorin, J. D., Paul, A. S., Madugundu, A. K., Gilberger, T., Gowda, H., Duraisingh, M. T., Keshava Prasad, T. S., & Sharma, P. (2017). PfCDPK1 mediated signaling in erythrocytic stages of Plasmodium falciparum. *Nature Communications*, *8*(1). https://doi.org/10.1038/S41467-017-00053-1

Liang, Q. L., Nie, L. B., Li, T. T., Elsheikha, H. M., Sun, L. X., Zhang, Z. W., Zhao, D. Y., Zhu, X. Q., & Wang, J. L. (2022). Functional Characterization of 17 Protein Serine/Threonine Phosphatases in Toxoplasma gondii Using CRISPR-Cas9 System. *Frontiers in Cell and Developmental Biology*, *9*, 738794. https://doi.org/10.3389/FCELL.2021.738794/BIBTEX

Miranda-Saavedra, D., Gabaldón, T., Barton, G. J., Langsley, G., & Doerig, C. (2012). The kinomes of apicomplexan parasites. *Microbes and Infection*, *14*(10), 796–810. https://doi.org/10.1016/j.micinf.2012.04.007

Neye, H. (2007). Peptidyl - Prolyl Isomerases. *XPharm: The Comprehensive Pharmacology Reference*, 1. https://doi.org/10.1016/B978-008055232-3.60608-7

Pandey, K., Ferreira, P. E., Ishikawa, T., Nagai, T., Kaneko, O., & Yahata, K. (2016). Ca2+ monitoring in Plasmodium falciparum using the yellow cameleon-Nano biosensor. *Scientific Reports*, *6*. https://doi.org/10.1038/SREP23454

Patel, A., Perrin, A. J., Flynn, H. R., Bisson, C., Withers-Martinez, C., Treeck, M., Flueck, C., Nicastro, G., Martin, S. R., Ramos, A., Gilberger, T. W., Snijders, A. P., Blackman, M. J., & Baker, D. A. (2019). Cyclic AMP signalling controls key components of malaria parasite host cell invasion machinery. *PLoS Biology*, *17*(5). https://doi.org/10.1371/JOURNAL.PBIO.3000264

Paul, A. S., Miliu, A., Paulo, J. A., Goldberg, J. M., Bonilla, A. M., Berry, L., Seveno, M., Braun-Breton, C., Kosber, A. L., Elsworth, B., Arriola, J. S. N., Lebrun, M., Gygi, S. P., Lamarque, M. H., & Duraisingh,

M. T. (2020). Co-option of Plasmodium falciparum PP1 for egress from host erythrocytes. *Nature Communications*, *11*(1). https://doi.org/10.1038/S41467-020-17306-1

Paul, A. S., Saha, S., Engelberg, K., Jiang, R. H. Y., Coleman, B. I., Kosber, A. L., Chen, C.-T., Ganter, M., Espy, N., Gilberger, T. W., Gubbels, M.-J., & Duraisingh, M. T. (2015). Parasite Calcineurin Regulates Host Cell Recognition and Attachment by Apicomplexans. *Cell Host & Microbe*, *18*(1), 49–60. https://doi.org/10.1016/j.chom.2015.06.003

Perrin, A. J., Collins, C. R., Russell, M. R. G., Collinson, L. M., Baker, D. A., & Blackman, M. J. (2018). The Actinomyosin Motor Drives Malaria Parasite Red Blood Cell Invasion but Not Egress. *MBio*, *9*(4). https://doi.org/10.1128/MBIO.00905-18

Philip, N., & Waters, A. P. (2015). Conditional Degradation of Plasmodium Calcineurin Reveals Functions in Parasite Colonization of both Host and Vector. *Cell Host & Microbe*, *18*(1), 122–131. https://doi.org/10.1016/j.chom.2015.05.018

Steele, F. R., Washburn, T., Rieger, R., & O'tousa, J. E. (1992). Drosophila retinal degeneration C (rdgC) encodes a novel serine/threonine protein phosphatase. *Cell*, *69*(4), 669-676.

Tewari, R., Straschil, U., Bateman, A., Böhme, U., Cherevach, I., Gong, P., Pain, A., & Billker, O. (2010). The systematic functional analysis of Plasmodium protein kinases identifies essential regulators of mosquito transmission. *Cell Host & Microbe*, *8*(4), 377–387. https://doi.org/10.1016/J.CHOM.2010.09.006

Toenhake, C. G., Fraschka, S. A. K., Vijayabaskar, M. S., Westhead, D. R., van Heeringen, S. J., & Bártfai, R. (2018). Chromatin Accessibility-Based Characterization of the Gene Regulatory Network Underlying Plasmodium falciparum Blood-Stage Development. *Cell Host & Microbe*, *23*(4), 557-569.e9. https://doi.org/10.1016/J.CHOM.2018.03.007

Ward, P., Equinet, L., Packer, J., & Doerig, C. (2004). Protein kinases of the human malaria parasite Plasmodium falciparum: The kinome of a divergent eukaryote. *BMC Genomics*, *5*.

https://doi.org/10.1186/1471-2164-5-79

Wilkes, J. M., & Doerig, C. (2008). The protein-phosphatome of the human malaria parasite Plasmodium falciparum. *BMC Genomics*, *9*. https://doi.org/10.1186/1471-2164-9-412

Zhang, M., Wang, C., Otto, T. D., Oberstaller, J., Liao, X., Adapa, S. R., Udenze, K., Bronner, I. F., Casandra, D., Mayho, M., Brown, J., Li, S., Swanson, J., Rayner, J. C., Jiang, R. H. Y., & Adams, J. H. (2018). Uncovering the essential genes of the human malaria parasite Plasmodium falciparum by saturation mutagenesis. *Science (New York, N.Y.)*, *360*(6388). https://doi.org/10.1126/SCIENCE.AAP7847

Zhu, X., Li, S., Wang, C., Yu, Y., Wang, J., He, L., Siddiqui, F. A., Chen, L., Zhu, L., Zhou, D., Qin, J., Miao, J., Cui, L., & Cao, Y. (2022). The Plasmodium falciparum Nuclear Protein Phosphatase NIF4 Is Required for Efficient Merozoite Invasion and Regulates Artemisinin Sensitivity. *MBio*, *13*(4). https://doi.org/10.1128/mbio.01897-22

Figure 1

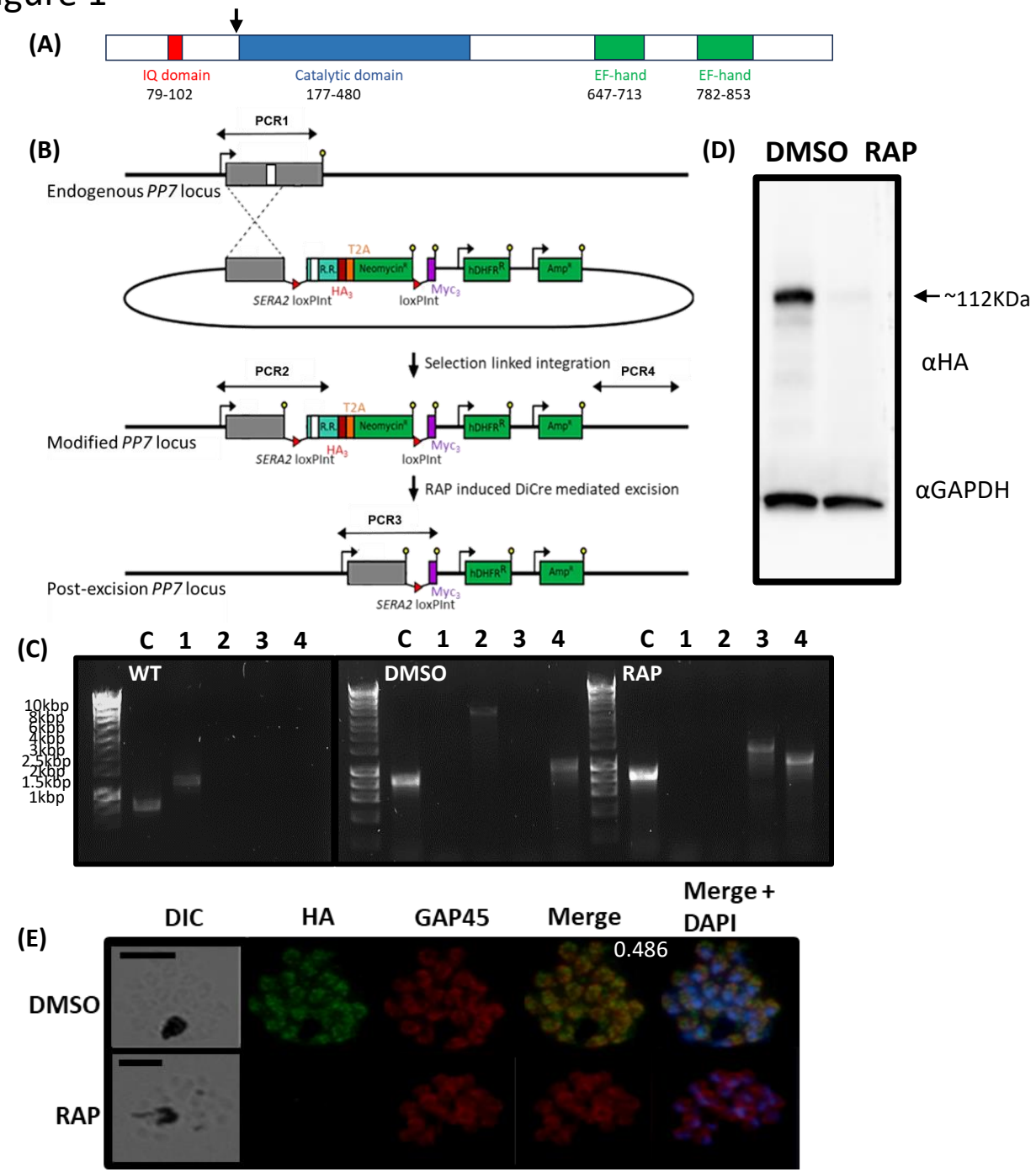

(1A) Cartoon of the predicted *P. falciparum* PP7 protein showing the positions of the individual domains. Amino acid numbers are shown in black. The arrow indicates the point at which the protein product is truncated when the modified locus is excised in the transgenic parasites.

(1B) Schematic representation of the SLI strategy (57) used to produce the PP7-HA:loxP DiCre line and resultant RAP-induced disruption of the modified gene. Double-headed arrows represent the regions amplified by PCR in (1C). Red arrowheads represent *loxP* sites, yellow lollipops represent translational stop codons, white box indicates the metallo-dependent phosphatase domain, light blue box indicate regions of re-codonised sequence (R.R.).

(1C) Diagnostic PCR analysis of gDNA from a transgenic PP7 parasite line verifying successful modification of target loci by SLI to produce PP7-HA:loxP. Efficient excision of 'floxed' sequences is observed upon treatment with RAP. Track C represents amplification of a control locus (PKAr) to check gDNA integrity. PCRs 1-4 are represented in the schematic locus in panel 1B. PCR 1 screens for the WT locus, PCR 2 for 5' integration, PCR 3 for the excision of the 'floxed' sequence and PCR 4 for 3' integration . See Table 1 for sequences of all primers used for PCR. Sizes for expected amplification products are as follows: C, control locus (primers 5 and 6) 836 b.p. PCR 1 (primers 7 and 8) 1296 b.p, PCR2 (primers 7 and 9) 3559 b.p, PCR3 (primers 7 and 10) 1362 b.p. (RAP) and PCR 4 (primers 11 and 8) 1013 b.p.

(1D) Western blot analysis of expression (DMSO) and ablation (RAP) of PP7-HA from highly synchronous late stage schizonts. Expression of GAPDH (PF3D7_1462800) is shown as a loading control.

(1E) IFA analysis showing the diffuse peripheral localisation of PP7-HA and the loss of expression upon RAP treatment (16 hours post invasion). GAP45 was sued as a marker of the parasite IMC, 0.486 inset number is the Pearson correlation coefficient of co-localisation. Over 99% of all RAP-treated PP7-HA:loxP schizonts examined by IFA were diminished in HA expression in three independent experiments. Scale bars, 2 µm.

Figure 2

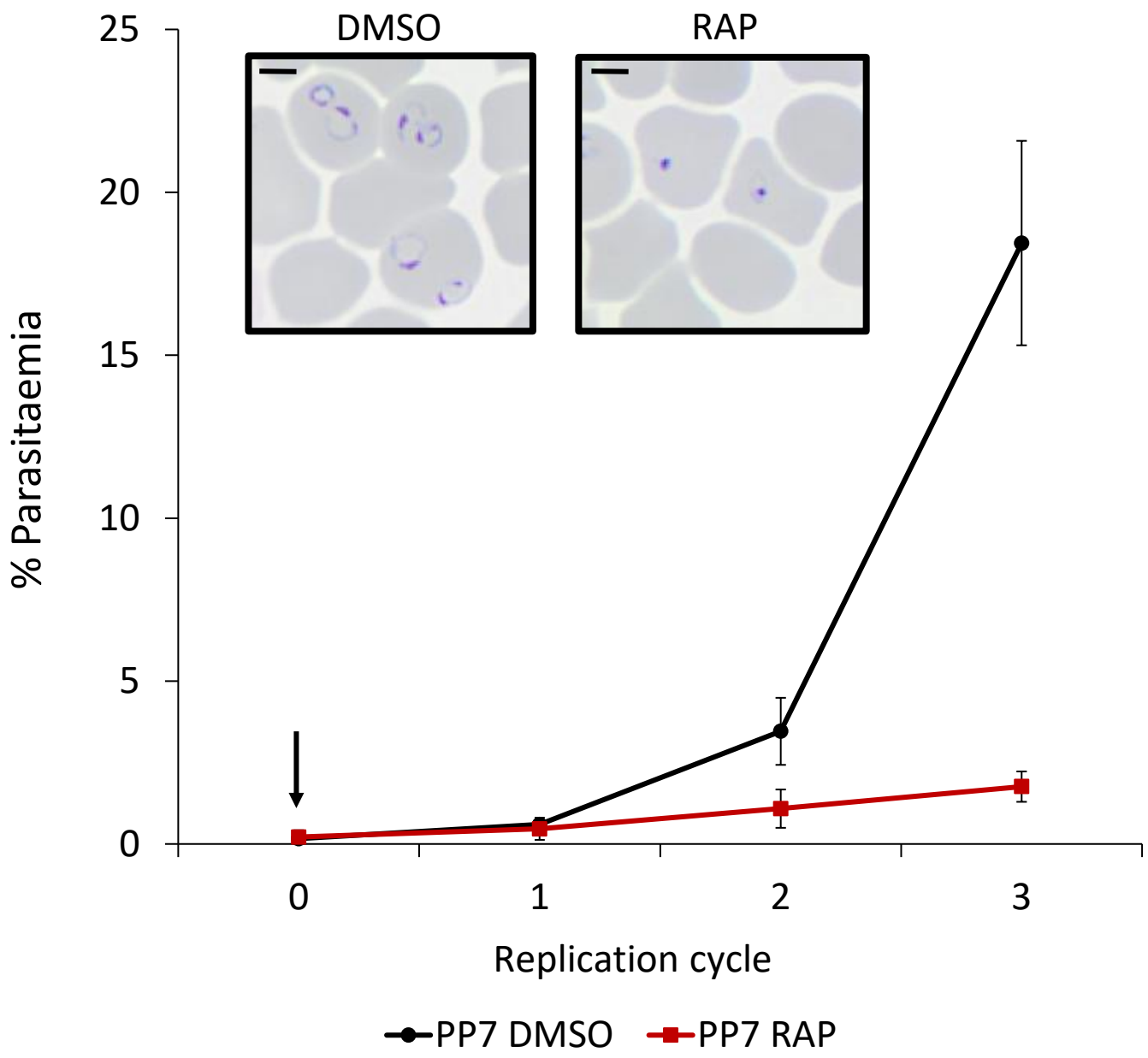

Growth curves showing parasitaemia as measured by flow cytometry of PP7-HA:loxP parasites treated with DMSO (vehicle only control) or RAP, vertical arrow indicates treatment point. Means from 2 independent biological replicates are plotted. Error bars, SD. Inset, Giemsa-stained thin blood films showing ring-stage parasites following egress of synchronous DMSO and RAP-treated PP7-HA:loxP schizonts. Ring formation occurs in DMSO-treated PP7-HA parasites, parasites did not develop beyond the early ring stage in RAP-treated parasites. Scale bars, 2 µm.

Figure 3

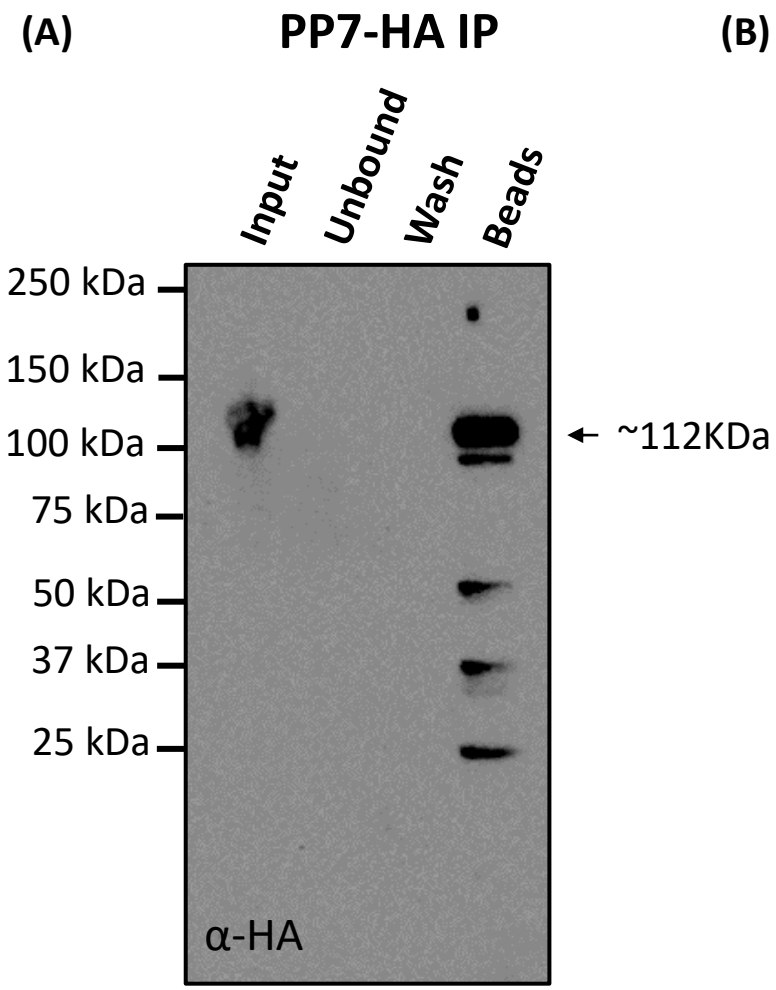

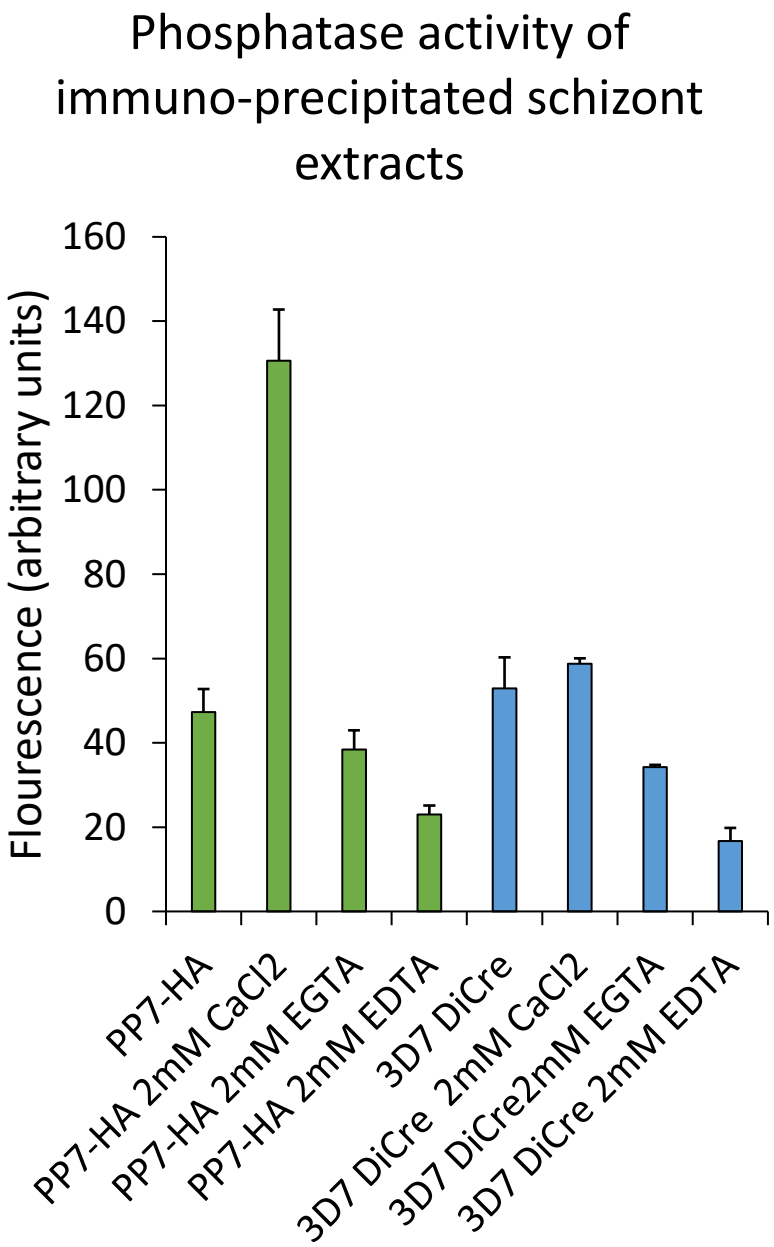

(3A) Western blot demonstrates efficient immunoprecipitation (IP) of PP7-HA from schizont extracts. Large black arrows indicate the predicted mass of PP7-HA, some lower molecular weight degradation products are visible. Images are representative of 2 independent biological repeats.

(3B) Phosphatase assay of immuno-precipitated PP7-HA conjugated beads. PP7 conjugated bead conditions are shown in green and control beads from 3D7 DiCre parental schizont lysate immuno-precipitation are displayed in blue. Results are averages of 3 independent biological repeats.

Figure 4

(A)

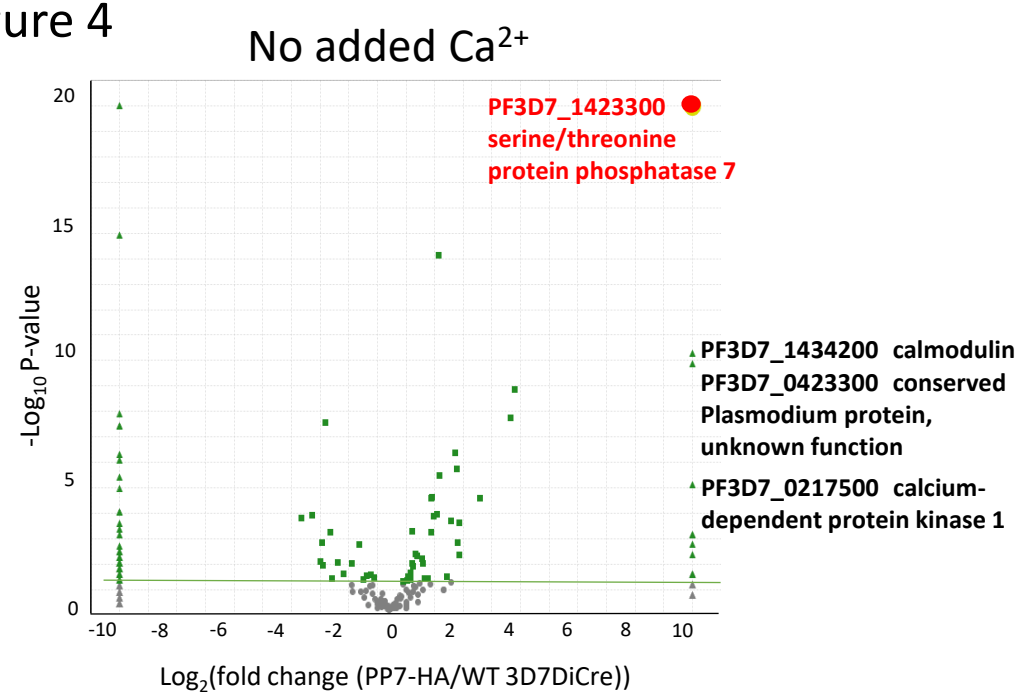

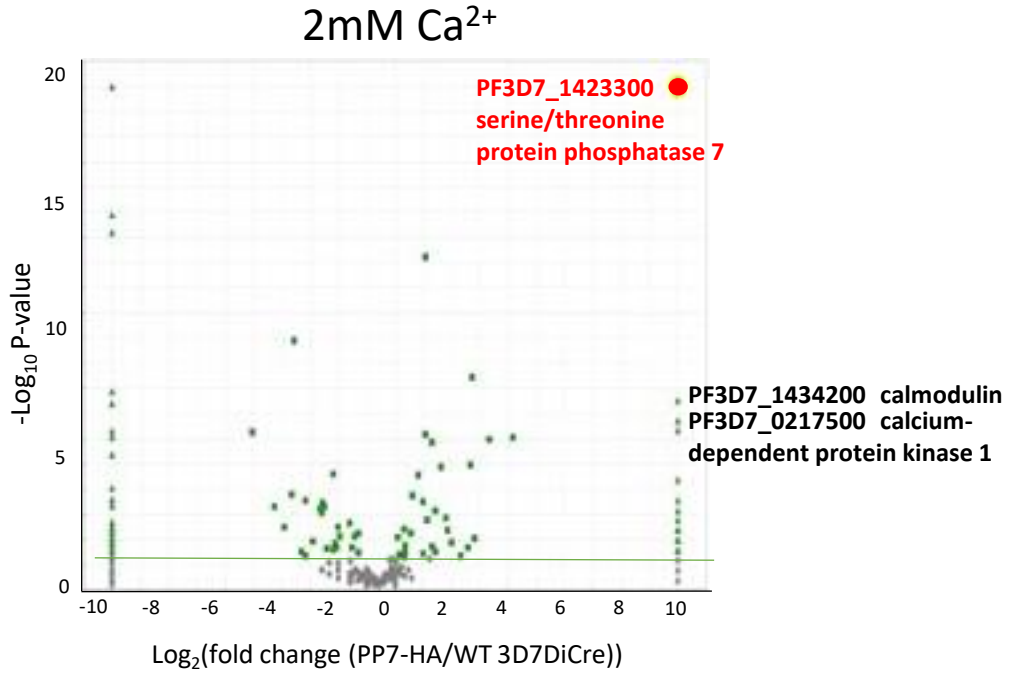

(B)

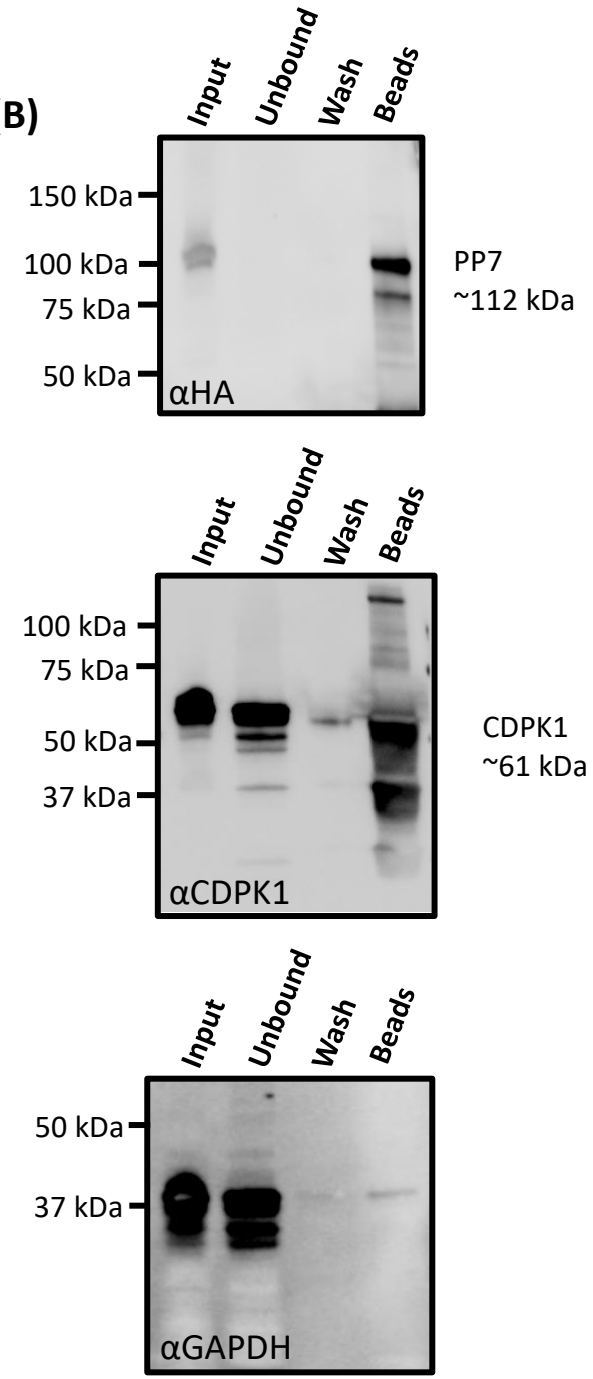

(4A) Mass spectrometric identification of interacting partners of PP7. Right panel shows immuno-precipitation with no added Ca^{2+} ions, left panel shows immuno-precipitation in the presence of additional 2mM Ca^{2+}. Volcano plot of P values versus the corresponding log_2 fold change in abundance compared to 3D7DiCre control samples (Fischer's exact test). Plotted by analysing proteins enriched through IP (panel 3A) by mass spectrometry. Green line indicates p=-$2log_{10}$ and green dots represent peptides where p<-$2log_{10}$. Peptides for PP7 were enriched to p<-$19log_{10}$.

(4B) Western blot analysis of immuno-precipitated PP7:HA-loxP schizont lysates confirms co-precipitation of CDPK1 when PP7-HA is affinity purified with anti HA beads. GAPDH is used as a cytosolic marker negative control to account for non-specific binding.

Figure 5

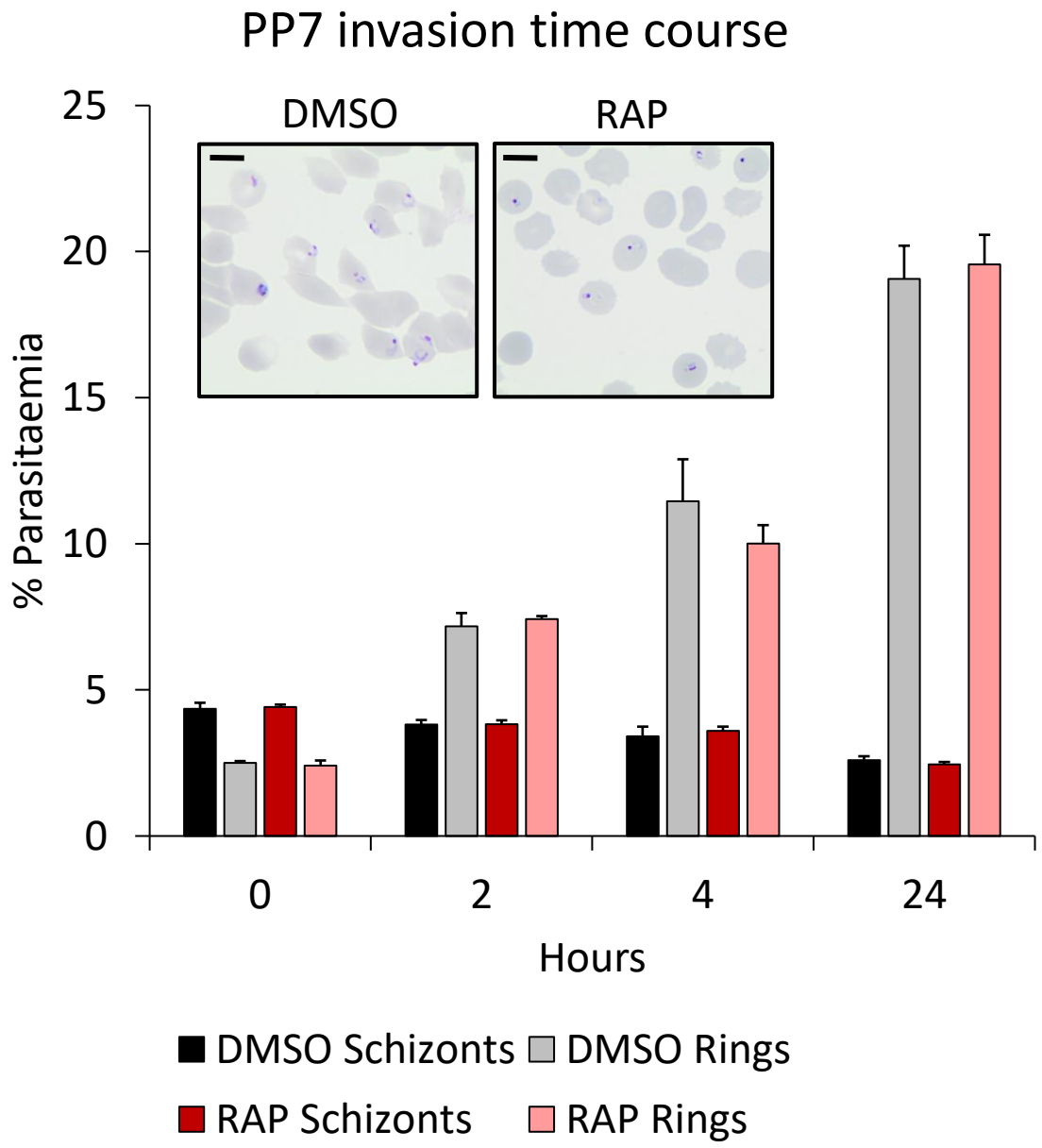

Flow cytometry analysis of ring formation in DMSO- and RAP-treated PP7-HA:loxP parasites treated in the previous cycle. Samples from highly-synchronized cultures treated at the ring stage the cycle prior to invasion and analysis, were taken in triplicate at the stated time intervals post invasion and stained with the DNA stain SYBR green. Samples were analyzed by flow cytometry, and the schizont and ring parasitemia values determined by gating high-signal and low-signal SYBR-positive cells, respectively. Mean parasitemia values (starting schizontemia adjusted to 2%) from two independent experiments are plotted. Error bars, SD; Insets are smears taken from cultures at 24h post invasion. Scale bars, 5 µm.

Figure 6

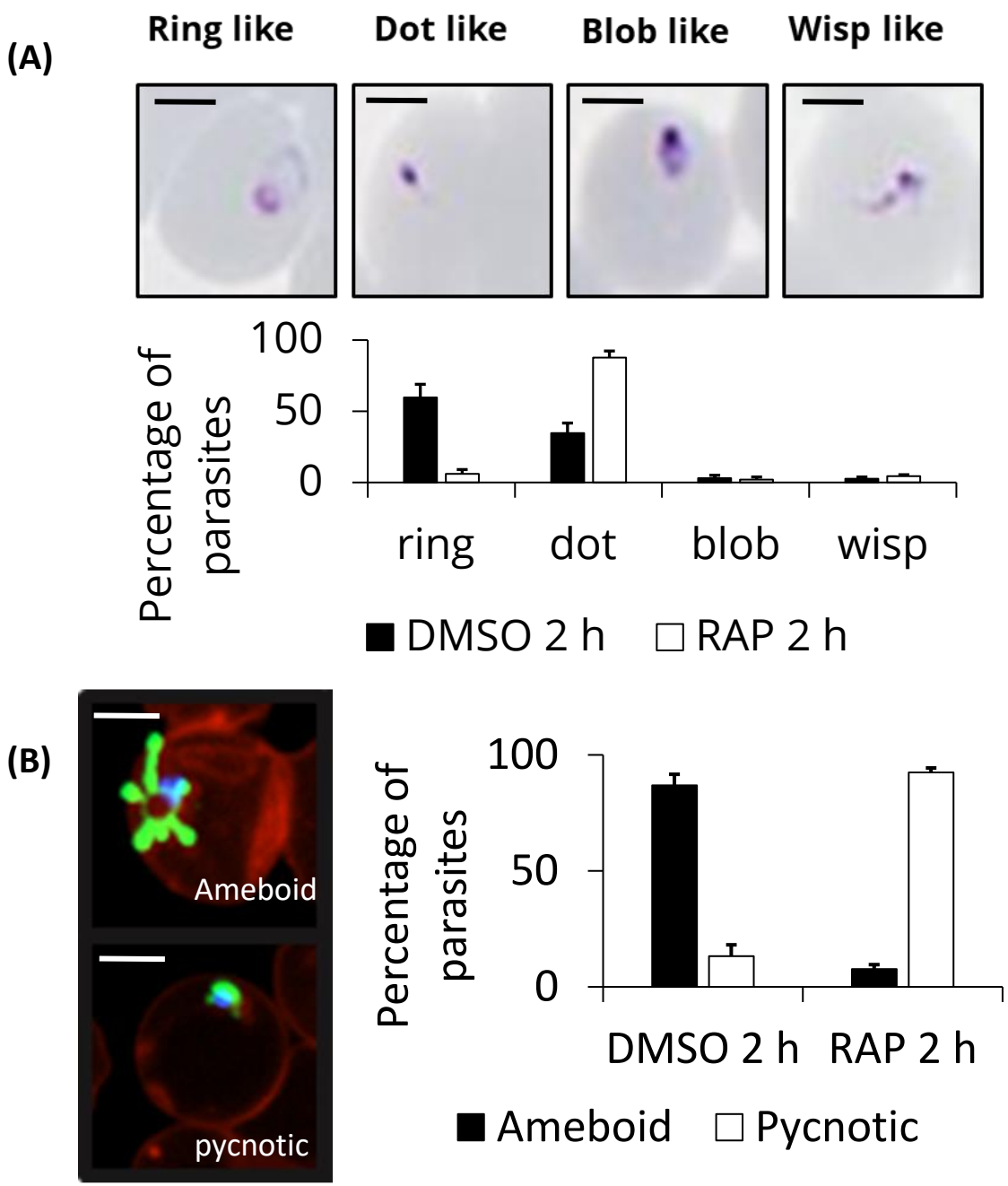

Effects of PP7 ablation on ring stage parasite development. (A) Tightly synchronized DMSO- or RAP-treated PP7-HA:loxP parasites were held in a C2 block until 48hr PI and subsequently washed and left to invade in fresh pre-warmed medium, after 2 hours thin blood smears were taken, and Giemsa stained. Ring stage parasite morphology was classified by manual counting. A minimum of 100 cells were counted per replicate and scored for morphology, scale bar 2 µm. (B) Tightly synchronized DMSO- or RAP-treated PP7-HA-Cyto-mNeon:loxP parasites were held in a C2 block until 48hr PI and subsequently washed and left to invade in fresh pre-warmed medium, parasites were then stained with BODIPY TR ceramide and Hoechst 3342 to visualise membranes and nuclei, respectively. Parasite samples were placed in an Ibid chamber slide and imaged by fluorescence microscopy. A minimum of 40 ring stage cells were counted per condition and scored for ameboid or pycnotic morphology of parasites, scale bar 2 µm. Mean data are plotted for three independent experiments. Error bars, SD, * $P<0.05$, Student's t test for the comparison of conditions between DMSO and RAP treatments.

Figure 7

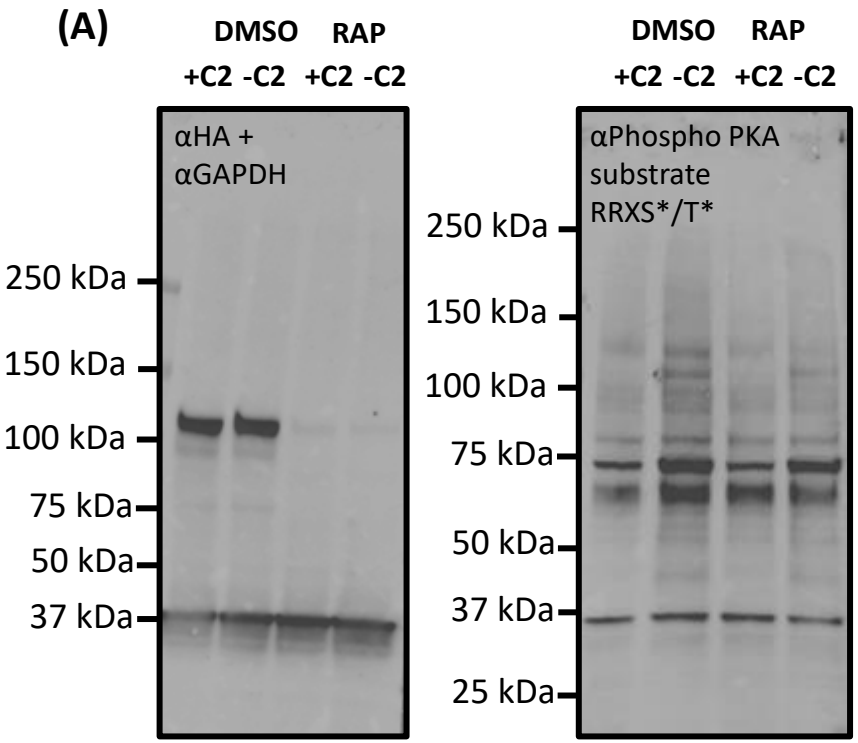

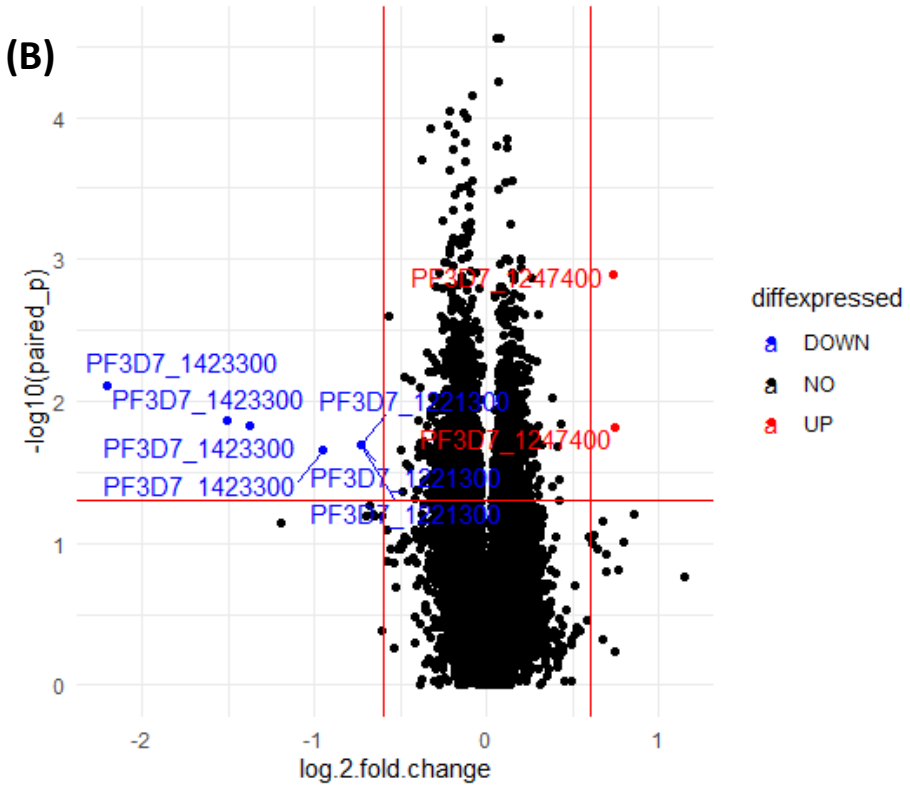

(7A) Tightly synchronized DMSO- or RAP-treated PP7-HA:loxP parasites were held in a C2 block until 48hr post invasion and half of the sample harvested for western blot analysis (+C2). The remainder of cells were washed with per-warmed medium to remove C2 and left to rupture for 20 minutes before harvesting (-C2). Sampels were analysed for ablation of PP7 and sample loading by probing with anti-HA and GAPDH antibodies respectively (left panel). A duplicate loading was probed to identify the abundance and patterning of phosphorylated PKA substrate motifs by probing with an anti-phospho PKA substrate antibody, which detects the motif RRXS*/T*, where S* and T* are phosphorylated serine and threonine residues respectively.

(7B) Volcano plot showing the changes in detection of phosphosites between DMSO- and RAP-treated PP7-HA:loxP. The negative log10 transform of the p-value–derived Welch-corrected t test comparing five DMSO- and five RAP-treated replicates is plotted against the log2-transformed fold change in reporter ion intensity (DMSO/RAP). Significance of $p < 0.05$ is denoted by the horizontal line. Vertical lines indicate –0.7 and 0.7 log2 fold change. Points labelled in blue are signifcantly down regulated, points in red significantly up-regulated.